Soft Matter

PAPER

View Article Online
View Journal | View Issue

Cite this: *Soft Matter*, 2026, 22, 1183

Moisture sorption of cellulose-based porous media containing co-solvents and its impact on pore-fiber transport rates of co-solvent solutions

Sajjad Karimnejad and Anton A. Darhuber *

Received 21st August 2025,
Accepted 21st December 2025

DOI: 10.1039/d5sm00847f

rsc.li/soft-matter-journal

Water-based inkjet inks typically contain non-volatile, polar compounds – referred to as co-solvents – such as glycerol and ethylene glycol oligomers, which constitute approximately 5–50 wt% of the total ink. The hygroscopic nature of both paper and co-solvents makes their interplay with atmospheric moisture a critical factor in controlling the penetration and drying dynamics of ink, as well as the long-term mechanical and morphological stability of the printed paper. In this study, we systematically investigate how co-solvent deposition influences equilibrium moisture uptake and how the ambient humidity influences the ink absorption dynamics into cellulose fibers. We find that co-solvent addition substantially increases moisture uptake and eliminates the sorption hysteresis present in paper. The moisture sorption of co-solvent-infused paper is well-predicted by the mass-weighted average of the individual, single-material sorption isotherms of paper and co-solvent. The rate of pore-fiber transport of co-solvents was observed to depend sensitively on ambient humidity, the presence of predeposited liquids as well as the addition of surfactants and divalent salts.

1. Introduction

Inkjet printing is a non-contact digital deposition technique widely used in both graphic applications and functional device manufacturing due to its high resolution, scalability, and flexibility regarding ink composition.[1–3] To ensure optimum performance, critical factors such as ink properties, ink–substrate interactions, and environmental conditions must be carefully controlled. Specifically, fluctuations in ambient relative humidity (RH) and temperature can significantly impact print quality.[4–8]

Cellulose-based paper, exhibiting biocompatibility and mechanical flexibility, constitutes the default substrate for a range of printing applications. Paper is a hygroscopic material. Its moisture content (defined as the ratio of the moisture mass absorbed by a paper sheet to its dry mass) responds dynamically to variations in ambient relative humidity and temperature.[9–15] Moisture uptake strongly affects the mechanical properties of paper such as its stiffness.[14,16–19] Moreover, paper is an anisotropic material, which exhibits non-uniform hygroexpansion.[20–22] Spatial gradients in moisture content can induce morphological instabilities such as curl, cockling, and multi-directional sheet distortions.[23–29]

Water-based inks are widely used in inkjet printing.[30] The main ingredients are water (30–90 wt%) and a co-solvent such as glycerol or ethylene glycol oligomers (EGOs, 5–50 wt%), along with several other components such as surfactants and colorants.[31] Co-solvents are polar, hygroscopic liquids with low vapor pressure that are added to prevent nozzle clogging in inkjet systems.[32]

After ink deposition and drying, the presence of residual co-solvent within the paper matrix can significantly alter its moisture sorption behavior. The affinity of co-solvents for the cellulose fibers potentially modifies their capacity to absorb and retain moisture. As a result, the sorption isotherm, which represents the equilibrium relation between moisture content and relative humidity, will change. The impact of EGOs on the hygroscopic response of wood – a closely related material system – was found to depend on the molecular weight of the EGO molecules and their specific location within the wood matrix.[33] Shomali *et al.* observed that addition of EGOs reduces the overall moisture sorption capacity.[34] In contrast, Saberi *et al.* found that starch films containing glycerol absorbed more moisture at all RH levels.[35]

While the moisture sorption properties of paper and co-solvents have been studied independently,[10,12,36,37] the behavior of co-solvent-infused paper regarding moisture uptake remains largely unexplored. Given the strong dependence of paper properties on the moisture content and the hygroscopic nature of co-solvents, it is critical to understand the response of

Fluids & Flows Group, Department of Applied Physics, Eindhoven University of Technology, Postbus 513, 5600MB Eindhoven, The Netherlands.
E-mail: a.a.darhuber@tue.nl

the two-component system to varying humidity conditions relevant to inkjet printing. In this study, we address this gap by investigating two key aspects: (1) the effect of the presence of co-solvents in the paper matrix on the overall moisture sorption capacity and (2) the influence of relative humidity on the transport rates of co-solvents from the interfiber into the intrafiber pores ('pore-fiber transport').[28,38–40] These factors are central to understanding the drying dynamics and to controlling print quality and its long-term stability in inkjet printing applications.

We built two experimental setups to study these aspects under controlled environmental conditions. To ensure the generality of our results, two different commercial printing papers and one laboratory-grade filter paper were used. We propose a model that reproduces the measured moisture sorption behavior of the two-component system of paper/co-solvents well over a broad range of water activities, for different co-solvents and different paper types. Furthermore, we systematically investigated the influence of the initial moisture and the initial co-solvent content on the pore-fiber transport dynamics of model inks. In addition to inkjet printing, our results are relevant to chromatography applications using paper substrates,[41] paper-based sensors,[42] paper microfluidics,[43] absorbent technology,[44] and the conservation of wood using co-solvents.[34]

2. Materials and methods

2.1. Materials and material properties

As co-solvents we used ethylene glycol (EG), tetra(ethylene glycol) (TEG), poly(ethylene glycol) with an average molecular weight (MW) of 300 (PEG300), and glycerol. PEG300 and glycerol were specifically selected for the sorption isotherm experiment due to their low vapor pressures of ≤ 14 μPa (PEG300)[45] and (13 ± 5) mPa (glycerol) at 20 °C,[46] which render them essentially non-volatile at room temperature. All chemicals were purchased from Sigma-Aldrich and used as received. The relevant material properties of the pure co-solvents are listed in Table S1 in the SI. Deionized water (Millipore, Direct-Q3 R) is used for rehydration and the preparation of aqueous co-solvent solutions.[28,38] For some experiments we used the anionic surfactant sodium dodecyl sulfate (SDS, Sigma-Aldrich, 436143) and the divalent metal salt $MgCl_2$ (Sigma-Aldrich, M8266).

As substrates we used the following uncoated, uncalendered and unsized paper types:

- Paper 'A': DNS high-speed inkjet natural feel paper (Mondi, grammage $g_A = 80$ g m^{-2} and thickness $d_{sub} = 104$ μm),
- Paper 'B': Z-Plot 650 paper (Ziegler, $g_B = 90$ g m^{-2} and $d_{sub} = 116$ μm),
- Paper 'C': Whatman filter paper, grade 44, diameter = 70 mm, $g_C = 80$ g m^{-2}, $d_{sub} = 180$ μm, made from cotton linters, ashless.

Papers A and B contain approximately 20 wt% and 12 wt% of $CaCO_3$ filler particles, respectively. Paper C is filler-free. Hereafter, the term 'untreated' refers to paper in its as-received condition.

2.2. Equilibrium moisture sorption – sample preparation

The sample dimensions for papers A and B are 20 × 10 cm. For Paper C, three circular pieces with a diameter of 7 cm are used. For experiments involving co-solvent-free papers, the samples are utilized without any additional treatment. For the preparation of co-solvent-infused papers, an atomizer (Timbertech, Airbrush Kit ABPST06) is employed to spray the co-solvent evenly across the samples. After spraying, the papers are placed on a holder for a minimum of one hour to allow for homogenization of the co-solvent distribution. This is followed by two sequential rehydration steps using deionized water to facilitate complete pore-fiber transport of the co-solvent.[28,38] The quantity of water sprayed at each rehydration step corresponds approximately to half of the weight of the paper sample. The time interval between the rehydration steps was (50 ± 10) min to allow for drying. The measurements started no sooner than 90 min after the final rehydration step was completed.

2.3. Equilibrium moisture sorption – experimental setup

Fig. 1 shows a sketch of the experimental setup. The prepared paper sample is placed on a metal wire basket that is suspended from a precision balance (Mettler Toledo, XSR225DU) by a thin metallic wire inside a humidity-controlled chamber. The paper weight is recorded every 10 minutes using a PC connected to the balance. A humidifier (Cellkraft, P-10) controls the relative humidity in the chamber. A humidity meter (Extech, SDL500) logs the temperature and humidity in the chamber. The temperature is usually (21 ± 0.2) °C and is constant throughout the course of an experiment. Care was taken when transferring the paper to prevent co-solvent loss,

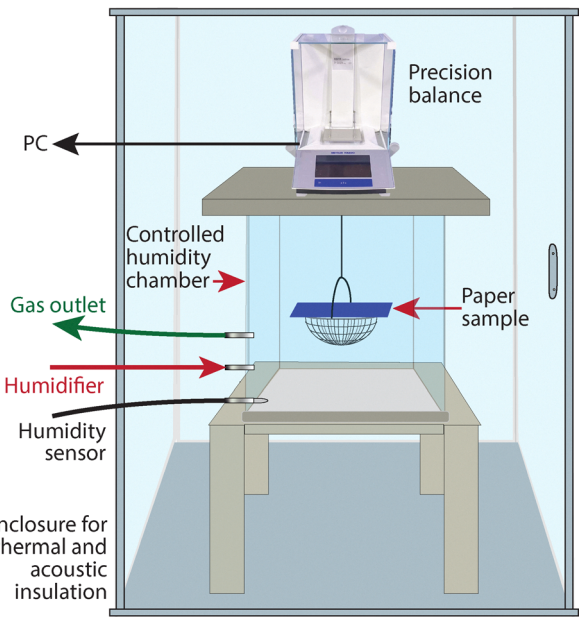

Fig. 1 Schematic of the experimental setup for measuring moisture sorption isotherms.

e.g., onto the wire-frame basket, on which the sample was placed. Adsorption isotherms were measured by incrementally increasing the relative humidity, followed by stepwise reduction of RH to record desorption isotherms.

2.4. Equilibrium moisture sorption – data analysis

To measure the mass of the dry paper m_p and the mass of the deposited co-solvent m_{cs}, samples are placed in the measurement chamber at zero humidity for a minimum of 48 hours. These parameters are determined using the following equations:

$$m_p = \text{mass(paper + basket + wire)} - m_b \quad (1)$$

$$m_{cs} = \text{mass(cs + paper + basket + wire)} - m_b - m_p \quad (2)$$

where m_b is the combined weight of the basket and its suspending wire. The co-solvent content θ_{cs} is defined as

$$\theta_{cs} = \frac{m_{cs}}{m_p} \quad (3)$$

and the total moisture content $(MC)_{total}$ is defined as

$$(MC)_{total} = \frac{m_{H_2O}}{m_p + m_{cs}} = \frac{m_{tot} - m_{cs} - m_p - m_b}{m_p + m_{cs}}, \quad (4)$$

where m_{tot} is the total mass recorded by the balance and m_{H_2O} is the mass of the absorbed moisture.

2.5. Paper swelling – sample preparation

For this experiment, samples of papers A and C with dimensions of 25 × 25 mm are used. For experiments without co-solvents, the samples are used as received. For the preparation of co-solvent-infused papers, an atomizer is employed to spray the co-solvent evenly across the samples. Subsequently, the papers are placed on a holder for a minimum of two hours to allow for homogenization of the co-solvent distribution. To prepare samples with an initial co-solvent content $\theta_{cs,ini}$ below or above 0.05 g g^{-1}, one or two sequential rehydration steps are performed using deionized water, respectively. The time interval between the rehydration steps was (30 ± 10) min to allow for drying. The measurements started no sooner than 2 h after the final rehydration step was completed.

2.6. Paper swelling – experimental setup

Fig. 2 shows a schematic of the experimental setup adapted from the study by Karimnejad *et al.*[40] A sheet of paper is maintained in an upright orientation by sandwiching it between two blackened metal holders underneath an upright microscope (Olympus BX50) with a 10× objective. The microscope is equipped with a CCD camera (Basler piA1000-60gm) and records the cross-sectional view of a paper sheet to monitor its thickness as a function of time. At the top of the metal holders, there is a recess (dimensions 5 × 5 mm^2), through which droplets of a model ink can be deposited onto the paper substrate using a digital syringe (Hamilton). All experiments were carried out at room temperature, (295 ± 2) K. The paper sample is enclosed in a chamber, the humidity of which is maintained at a constant level by a constant inflow of air from a humidifier (Cellkraft, P-10). A humidity meter logs the temperature and humidity in the chamber (Extech, SDL500).

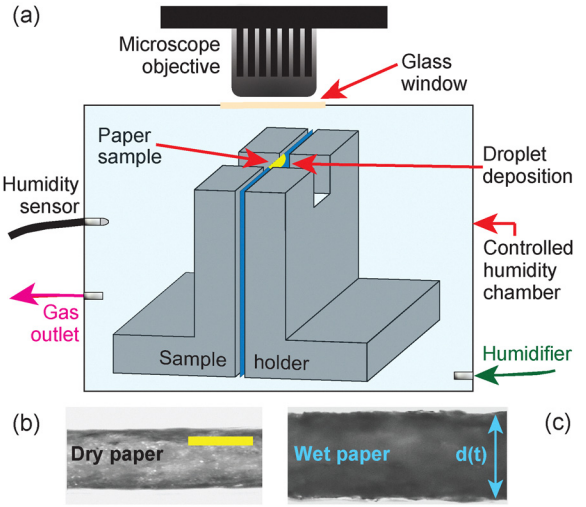

Fig. 2 (a) Schematic of the experimental setup for measuring paper swelling after deposition of co-solvent solutions as a function of relative humidity. (b and c) Representative top-view images of a (b) dry and (c) wet paper sheet. The scale bar in (b) corresponds to 100 μm.

3. Theoretical models

3.1. Equilibrium moisture sorption of untreated paper

The Guggenheim–Anderson–de Boer (GAB) isotherm

$$(MC)_{paper}(a_w) = \frac{M_0 C K a_w}{(1 - K a_w)(1 - K a_w + C K a_w)} \quad (5)$$

is a widely used empirical relation linking the equilibrium moisture content (MC) of a material and the ambient water activity defined as

$$a_w = \frac{p_{H_2O}}{p_{H_2O,sat}} \quad (6)$$

here, p_{H_2O} is the partial pressure of water vapor and $p_{H_2O,sat}$ is the saturated vapor pressure of water. The GAB isotherm has three adjustable parameters M_0, C and K. It is particularly well-suited for hygroscopic materials such as food products, pharmaceuticals, and cellulose-based materials such as paper.[10,47]

3.2. Equilibrium moisture sorption of co-solvents

The water activity a_w as a function of the composition of aqueous co-solvent solutions can usually be represented very accurately by the Van Laar equation[48,49]

$$a_w = x_w \exp\left[A_{21}\left(\frac{A_{12}(1 - x_w)}{A_{12}(1 - x_w) + A_{21}x_w}\right)^2\right], \quad (7)$$

where x_w is the mole fraction of water and A_{12} and A_{21} are adjustable parameters. The mole fraction of co-solvent is given by $x_{cs} = 1 - x_w$. The numerical values of the Van Laar fit parameters A_{12} and A_{21} for the co-solvents PEG300 and glycerol are provided in Table 1. For glycerol, we have fitted eqn (7) to

Table 1 Numerical values of the Van Laar fit parameters A_{12} and A_{21} for the co-solvents PEG300 and glycerol

Co-solvent	A_{12}	A_{21}
PEG300	−4.43	−0.5
Glycerol	−0.7	−0.3

the experimental data of Nakagawa and Oyama.[50] For PEG300, we resorted to interpolation between the experimental data in the studies by Eliassi *et al.*[51] and Ninni *et al.*,[37] as outlined in the SI.

From the mole fractions x_w and x_{cs}, we can obtain the weight fraction of the co-solvent

$$w_{cs} = \frac{(MW)_{cs} x_{cs}}{(MW)_{cs} x_{cs} + (MW)_w x_w} \quad (8)$$

as well as its equilibrium moisture content

$$(MC)_{cs} = \frac{1 - w_{cs}}{w_{cs}}. \quad (9)$$

The latter is plotted in Fig. 3(b) for glycerol and PEG300.

3.3. Equilibrium moisture sorption of the two-component system paper + co-solvent

There are three conceivable scenarios for equilibrium moisture sorption in the two-component system of co-solvent-infused paper:

1. The two materials do not interact in terms of moisture sorption, *i.e.* each material absorbs the same amount of water as if it were present in an isolated state. In this case, the sorption isotherm of the combined system is the linear superposition of the isotherms of the isolated systems.

2. The presence of co-solvent reduces the moisture sorption of cellulose, because a part of the polar surface sites of cellulose available for hydrogen-bonding with water are blocked by co-solvent molecules. In this case, the sorption capacity of the combined system is lower than the superimposed capacities of the isolated materials.

3. The presence of co-solvent plasticizes the paper substrate and causes significant swelling, which makes more sites available that can bind water molecules. In this case, the sorption capacity of the combined system is larger than the superimposed capacities of the isolated materials.

Furthermore, it is plausible that the location of the deposited co-solvent, *i.e.* whether it is contained in the micron-scale inter-fiber or the nano-scale intra-fiber pores,[28,38–40] makes a difference in which scenario is more likely to occur. Since moisture sorption in paper occurs primarily inside the cellulose fibers, scenario (1) is likely to occur if the co-solvent is contained in the inter-fiber pores. This is the case shortly after co-solvent deposition. In contrast, scenario (2) or (3) is potentially relevant to the equilibrium case, *i.e.* when the pore-fiber transfer of the co-solvent is complete and the co-solvent resides in the intra-fiber pores.

3.3.1. Non-interactive equilibrium moisture sorption of the two-component system paper + co-solvent. In the case of scenario (1), *i.e.* independent moisture sorption of the two materials, the total moisture content $(MC)_{total}$ is the mass-weighted average[52] of $(MC)_{paper}$ and $(MC)_{cs}$

$$(MC)_{total} = \frac{(MC)_{paper} g_{paper} + (MC)_{cs} \Theta_{cs}}{g_{paper} + \Theta_{cs}}. \quad (10)$$

here, g_{paper} is the grammage of dry paper (*i.e.* its mass per unit area, with units of g m^{-2}) and $\Theta_{cs} \equiv \theta_{cs} g_{paper}$ (*i.e.* the mass of co-solvent deposited per unit area of paper, with units of g m^{-2}).

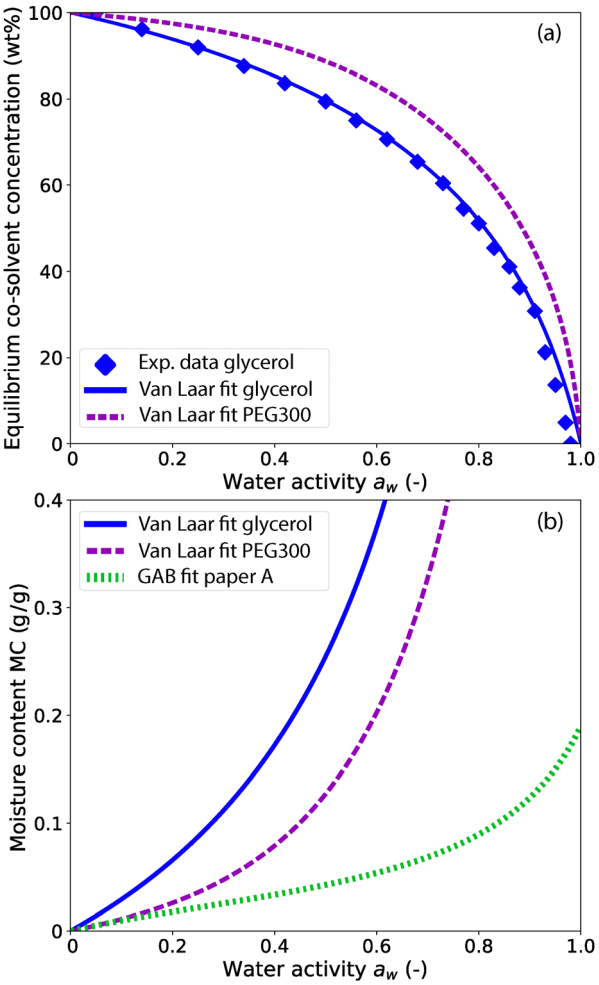

Fig. 3 (a) Equilibrium co-solvent concentration of glycerol and PEG300 as a function of water activity a_w for a temperature of 25 °C.[50] (b) Equilibrium moisture content as a function of a_w for glycerol (blue solid line) and PEG300 (purple dashed line). The green dotted line is a GAB fit for paper A.

4. Experimental results

4.1. Equilibrium moisture sorption and swelling of untreated paper

For every value of the water activity, 24 hours are allotted for moisture equilibration. The corresponding equilibrium moisture sorption isotherms for adsorption and desorption are shown in Fig. 4 as the filled and open symbols, respectively.

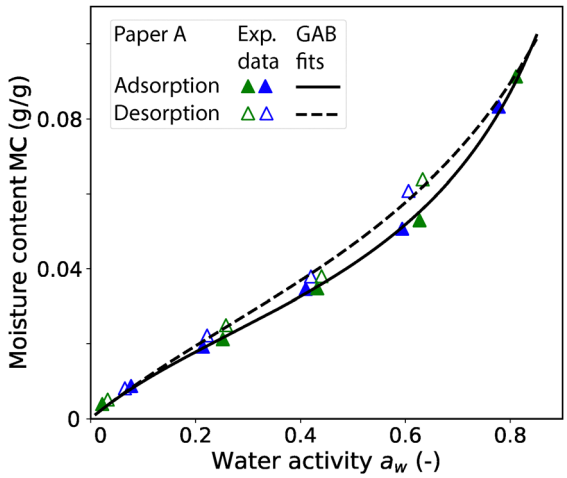

Fig. 4 Equilibrium moisture sorption isotherms for untreated paper A from two different experiments. Filled and open symbols represent the experimental data for adsorption and desorption, respectively. The solid and dashed lines are corresponding GAB fits.

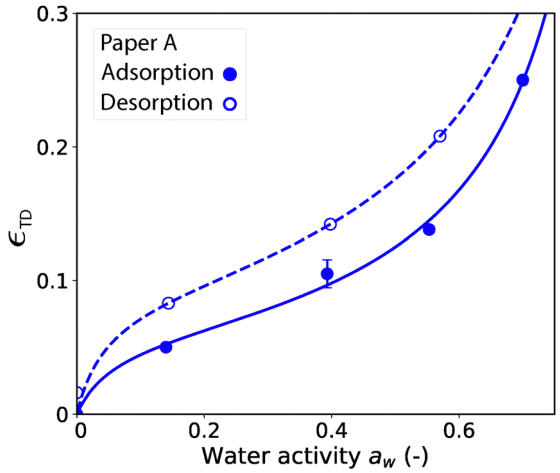

Fig. 5 Thickness expansion strain ε_{TD} of paper A as a function of water activity a_w. Filled and open symbols correspond to experimental data obtained for increasing and decreasing water activities, respectively. Solid and dashed lines are guides to the eye.

A representative sorption cycle is provided in Fig. S2 in the SI. To illustrate the reproducibility of the experiment, two independent datasets are shown for untreated paper A in blue and green. We performed GAB fits using eqn (5) of both the adsorption and desorption data, which are shown as the solid and dashed lines, respectively. Table 2 lists the numerical values of the corresponding GAB fit parameters. For all paper types, the MC on the adsorption curve (measured in the direction of increasing a_w levels) is always lower than that on the desorption curve (decreasing a_w levels). The moisture sorption is thus history-dependent and exhibits a small degree of hysteresis.

Fig. 5 shows the thickness hygroexpansion strain

$$\varepsilon_{TD} \equiv \frac{d - d_{dry}}{d_{dry}} \tag{11}$$

of untreated paper A as a function of a_w for increasing and decreasing water activities. Chen *et al.* found that there is no hysteresis in the expansion strain of amorphous cellulose, if it is plotted as a function of the moisture content.[53] In contrast, for paper A, we still observe considerable hysteresis in the correlation between ε_{TD} and MC, see Fig. S4(a) in the SI.

4.2. Equilibrium moisture sorption and swelling of co-solvent-infused paper

Fig. 6(a and c) shows the equilibrium moisture sorption isotherms for co-solvent-infused paper A. The filled and open symbols denote the adsorption and desorption branches, respectively. The solid and dashed lines represent eqn (10), *i.e.* the theoretical model according to scenario (1), where we substituted the adsorption/desorption GAB fits of Fig. 4 for $(MC)_{paper}$. Equivalent datasets for papers B and C, with the corresponding fit parameter values, are presented in Fig. S3 and Table S2 of the SI. The addition of co-solvents significantly increases the equilibrium moisture content and removes the hysteresis. Fig. 6(b) presents the scaled hysteresis amplitude

$$\frac{\Delta(MC)}{\langle MC\rangle} \equiv \frac{(MC)_{des} - (MC)_{ads}}{\frac{1}{2}\left[(MC)_{des} + (MC)_{ads}\right]} \tag{12}$$

of the paper A + PEG300 moisture sorption isotherms in Fig. 6(a) evaluated at $a_w = 0.5$. The values of $(MC)_{des}$ and $(MC)_{ads}$ were determined by interpolating the experimental data to $a_w = 0.5$ using GAB fits of the adsorption and desorption curves. Hysteresis disappears at $\theta_{cs} \approx 0.2$ g g^{-1}.

We also determined the influence of co-solvents on the correlation between the swelling amplitude and water activity a_w. Fig. S4(b) in the SI illustrates that – similar to the removal of moisture sorption hysteresis in Fig. 6(a and b) – the presence of approximately 0.2 g g^{-1} PEG300 suppresses the considerable expansion strain hysteresis observed with untreated paper A in Fig. 5.

Table 2 Numerical values of GAB fit parameters for paper A

	M_0	C	K
Adsorption	0.031	4.50	0.85
Desorption	0.042	3.60	0.75

4.3. Impact of initial moisture/co-solvent content on pore-fiber transport rates of aqueous co-solvent solutions

Following the study by Karimnejad *et al.*,[40] we monitored the swelling of a paper sheet in the thickness direction to characterize the pore-fiber transport of co-solvents. A paper sample was first equilibrated to a certain water activity for 24 h inside a humidity-controlled chamber at room temperature, after which we deposited a droplet (volume $V = 1$ μL) of an aqueous co-solvent solution. Fig. 7(a) shows typical results of the increment of the thickness expansion strain

$$\Delta\varepsilon_{TD} \equiv \frac{d(t) - d(t=0)}{d(t=0)} \tag{13}$$

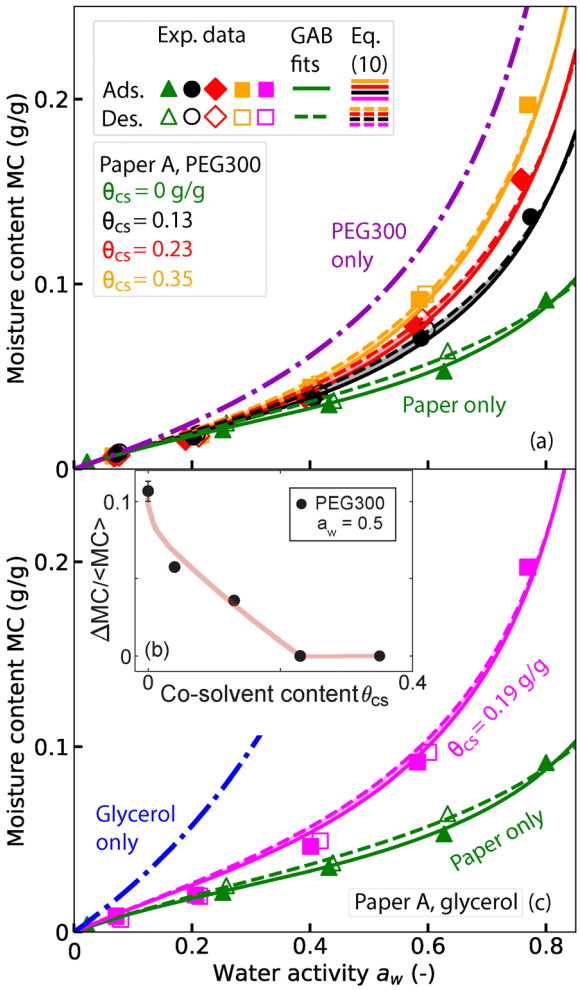

Fig. 6 Moisture sorption isotherms for paper A containing (a) PEG300 and (c) glycerol. Solid and open symbols denote the adsorption and desorption branches, respectively. Solid and dashed lines represent eqn (10), *i.e.* the theoretical model according to scenario (1). (b) Scaled hysteresis amplitude ΔMC/$\langle$MC$\rangle$ of the paper A + PEG300 isotherms at a_w = 0.5 as a function of PEG300 content. The solid line is a guide to the eye.

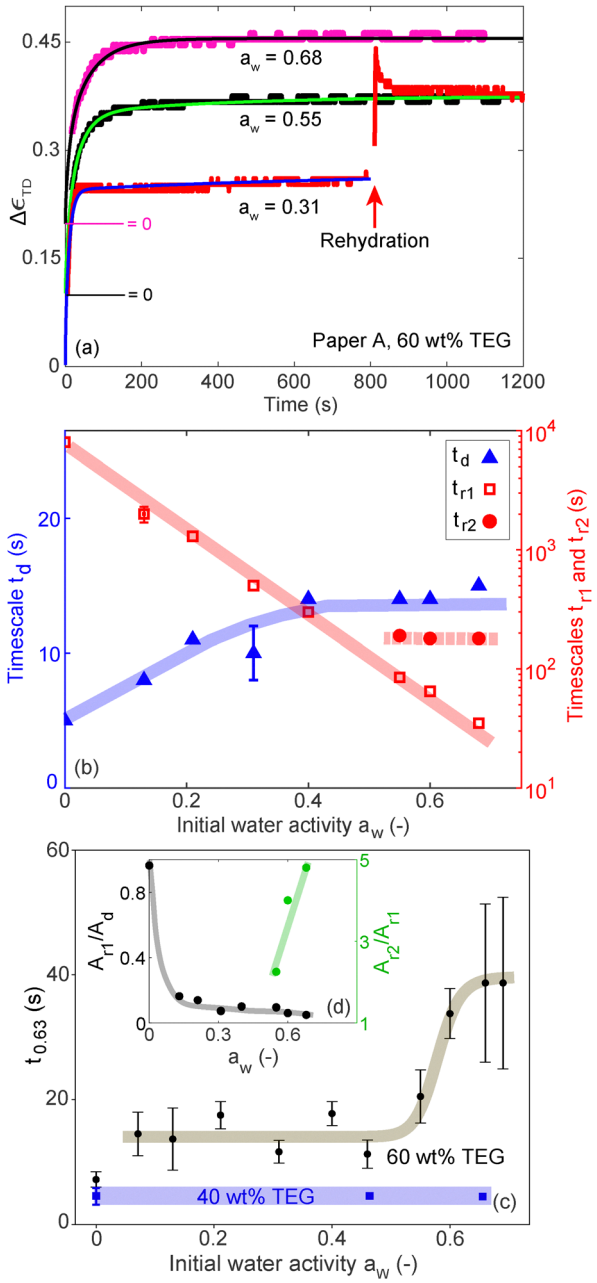

Fig. 7 (a) Increment of the thickness expansion strain $\Delta\varepsilon_{TD}$ of untreated paper A as a function of time after deposition of a droplet (V = 1 μL) of 60 wt% TEG for different values of a_w. The solid lines are fits according to the Berens and Hopfenberg model.[54] To aid visualization, the curves for a_w = 0.55 and 0.68 were shifted by 0.1 and 0.2 along the ordinate axis, respectively. (b) Corresponding diffusion and relaxation timescales t_d (triangles) and $t_{r1,2}$ (circles and squares) of untreated paper A as a function of initial water activity a_w. (c) Overall characteristic swelling timescale $t_{0.63}$ for solutions of TEG as a function of a_w. (d) Ratio of the strain amplitude factors A_{r1}/A_d and A_{r2}/A_{r1}. The solid lines in (b–d) are guides to the eye.

as a function of time for a 60 wt% TEG solution and different initial water activities a_w. Here, $d(t = 0)$ is the paper thickness just prior to deposition of the co-solvent solution (but after 24 h equilibration to a certain initial water activity a_w), which exceeds the thickness of dry paper d_{dry} due to hygroexpansion, see Fig. 5. The solid lines in Fig. 7(a) represent fits of the experimental data using the Berens and Hopfenberg (BH)[40,54] model that accounts for diffusive liquid uptake (with corresponding timescale t_d) as well as polymer relaxation (with timescales $t_{r1,2}$) – see Section VI in the SI.

A droplet of pure water (V = 1 μL) was added to the sample at $t \approx$ 800 s during the experiment for a_w = 0.31 to demonstrate the effect of rehydration.[38] The added water increases the local moisture content, decreases viscosity and acts as a plasticizer, promoting pore-to-fiber transport of the co-solvent and enabling the system to reach a higher value of ε_{TD}, *i.e.* closer to equilibrium.

Fig. 7(b) shows the resulting timescales t_d and $t_{r1,2}$ after deposition of a droplet of a 60 wt% TEG solution on paper A as a function of the initial water activity a_w. Interestingly, t_{r1} strongly decreases with increasing a_w, whereas t_d and t_{r2} show much less variation with a_w. Fig. 7(c) presents the corresponding overall characteristic swelling timescale $t_{0.63}$ for solutions of TEG as a function of the initial water activity a_w. $t_{0.63}$ is

defined as the time required for $\Delta\varepsilon_{TD}$ to reach 63% of its maximum value.[40] As $t_{0.63}$ does not result from curve-fitting, it is a more robust and universal characterization of the swelling dynamics. In contrast, t_d and $t_{r1,2}$ can be linked to different mechanisms or processes and thus contain more information, but their relevance is dependent on the success of the BH model in fitting the $\Delta\varepsilon_{TD}(t)$ data. In Fig. 7(d), we plot the ratios of the strain amplitude factors A_{r1}/A_d and A_{r2}/A_{r1} as functions of the initial water activity a_w.

Fig. 8(a) shows the increment of the thickness expansion strain $\Delta\varepsilon_{TD}$ of untreated paper A after deposition of a 1 μL droplet of pure EG as a function of the water activity. Fig. 8(b) presents the corresponding short diffusive timescale t_d and the longer relaxation timescale t_{r1} obtained from BH fits of the experimental data. Fig. 8(c) presents the corresponding overall characteristic swelling timescale $t_{0.63}$ as a function of water activity a_w. In contrast to the behavior of 60 wt% TEG in Fig. 7(b), t_d and $t_{0.63}$ for pure EG strongly and monotonically decrease with increasing a_w.

Fig. 9 shows the diffusion and relaxation timescales of paper A after deposition of a droplet (V = 1 μL) of pure EG as a function of the initial EG content of the paper sheet. This experiment mimics the case of inkjet printing a second time onto paper that already contains pre-existing ink patterns. Similar to Fig. 8(b), the swelling time for pure EG strongly and monotonically decreases with increasing $\theta_{cs,ini}$.

Fig. 9(c) shows the overall characteristic swelling timescale $t_{0.63}$ as a function of initial co-solvent (EG and glycerol) content

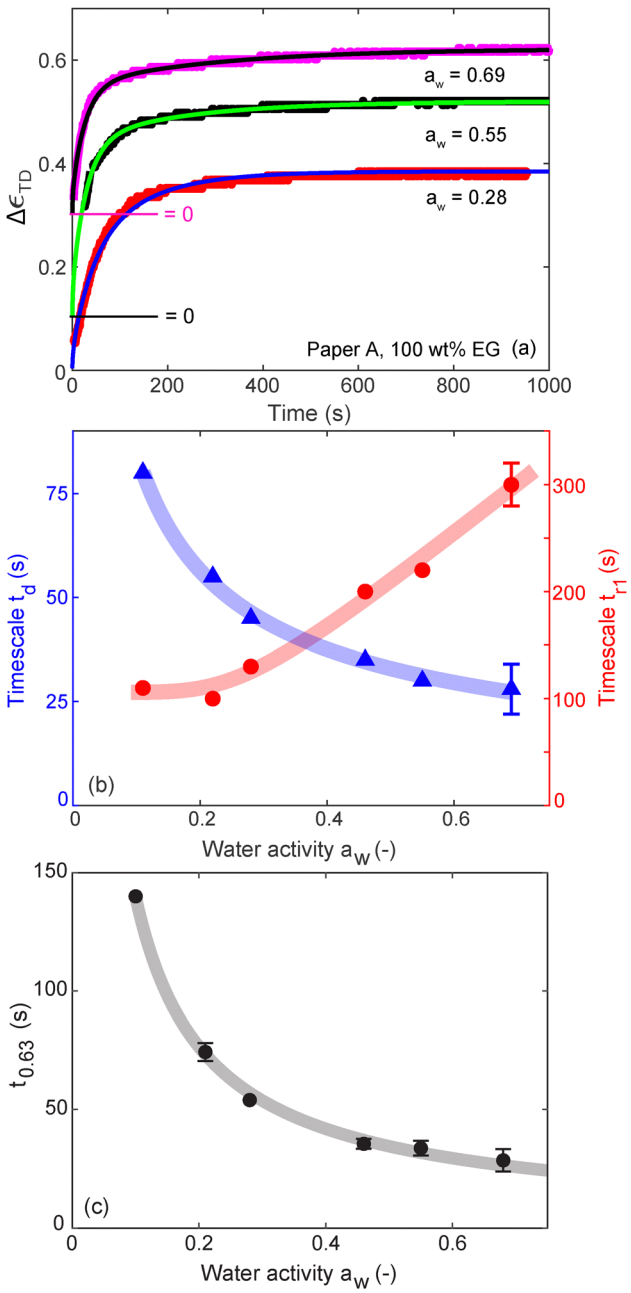

Fig. 8 (a) Increment of the thickness expansion strain $\Delta\varepsilon_{TD}$ as a function of time after deposition of pure EG droplets (V = 1 μL) on untreated paper A for different values of a_w. Solid lines are fits according to the BH model.[54] To aid visualization, the curves for a_w = 0.55 and 0.69 were shifted by 0.1 and 0.3 along the ordinate axis, respectively. (b and c) Corresponding diffusion and relaxation timescales t_d and t_{r1} and overall characteristic swelling timescale $t_{0.63}$ as functions of a_w. Solid lines in (b,c) are guides to the eye.

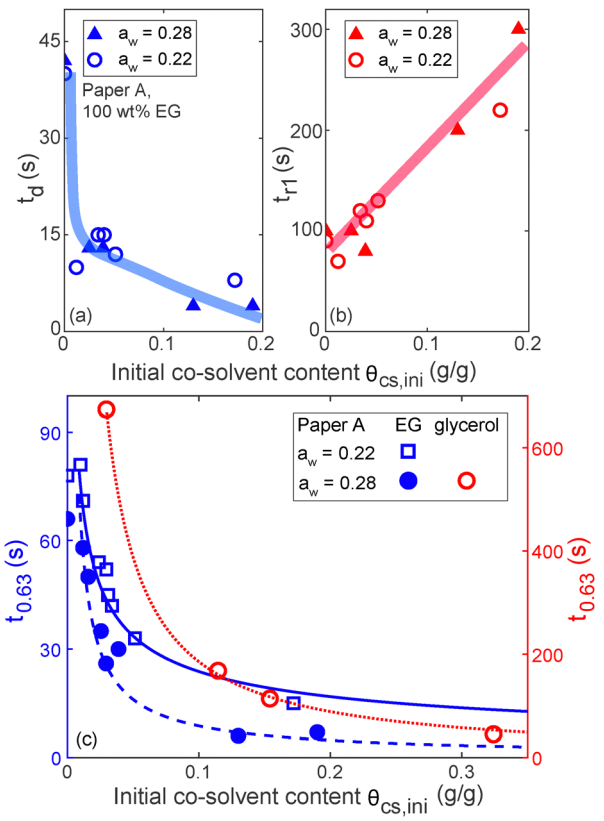

Fig. 9 (a) Diffusion timescale t_d and (b) relaxation timescale t_{r1} after deposition of a droplet (V = 1 μL) of pure EG on paper A as a function of initial EG content $\theta_{cs,ini}$ at two fixed water activities a_w = 0.22 (circles) and 0.28 (triangles). (c) Overall characteristic swelling timescale $t_{0.63}$ as a function of initial co-solvent content $\theta_{cs,ini}$ at fixed water activities of 0.22 (open squares) and 0.28 (circles). Blue symbols correspond to pure EG and red open circles to pure glycerol. All lines are guides to the eye.

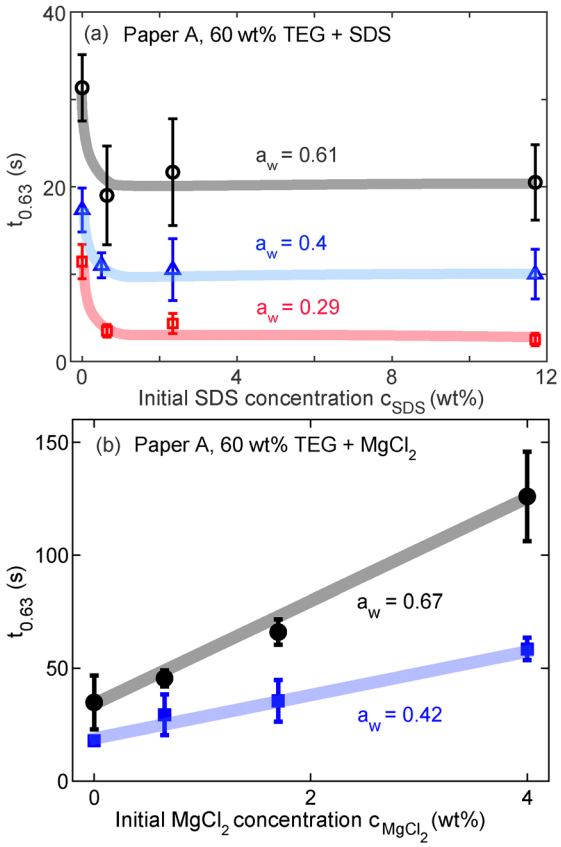

Fig. 10 Overall characteristic swelling timescale $t_{0.63}$ of paper A after deposition of a 1 μL droplet of a 60 wt% TEG solution containing either SDS or $MgCl_2$ as a function of (a) the initial SDS concentration c_{SDS} and (b) the initial $MgCl_2$ concentration c_{MgCl_2}, at different water activities a_w. Solid lines in (a and b) are guides to the eye.

$\theta_{cs,ini}$ at fixed water activities of a_w = 0.22 (open squares) and 0.28 (circles). A relatively minor increment in water activity Δa_w = 0.06 causes a significant reduction of $t_{0.63}$.

4.4. Impact of adding salt or surfactant on pore-fiber transport rates of aqueous co-solvent solutions

Fig. 10 shows $t_{0.63}$ of paper A after deposition of 60 wt% TEG containing the surfactant sodium-dodecyl-sulfate (SDS) or the divalent metal salt $MgCl_2$ at different water activities a_w. The addition of SDS induces a marked reduction of $t_{0.63}$ for all water activities a_w [Fig. 10(a)], reaching a nearly constant value above about 0.5 wt% SDS. In contrast, the addition of $MgCl_2$ causes a strong increase of $t_{0.63}$ for all water activities a_w studied [Fig. 10(b)]. For both SDS and $MgCl_2$, higher relative humidity values significantly slow down the swelling dynamics.

5 Discussion

5.1. Equilibrium moisture sorption of untreated paper

Water vapor primarily interacts with hydroxyl groups on the surfaces of cellulose microfibrils or within non-crystalline domains, while those located in crystalline regions remain largely inaccessible due to intra- and intermolecular hydrogen bonding.[55,56] According to Mihranyan *et al.*[57] and Ioelovich and Leykin,[58] the fraction of amorphous cellulose, *i.e.* its degree of crystallinity, has a major impact on its moisture sorption capacity, as it impacts the accessibility of polar groups such as hydroxyl and ether groups to water molecules.[36] Therefore, the composition and the details of the manufacturing process of paper have a significant influence on its moisture sorption capacity. Parker *et al.* showed that the moisture sorption capacity of pulp increases with beating and even more so with bleaching.[59] Bedane *et al.* showed that calendered paper types can have a 30% smaller moisture sorption capacity than uncalendered papers.[60] $CaCO_3$ filler particles are commonly added to printing paper, *e.g.*, to increase opacity and reduce cost. They tend to sorb much less water than cellulose.[61,62]

Although papers A and B contain approximately 12–20 wt% filler particles, their sorption capacities are higher than that of paper C, which is made purely from cotton linters. Since cotton contains a high level of crystalline cellulose and low levels of amorphous polysaccharide and nophenolic content,[36,63] it exhibits fewer accessible OH groups compared to other fibers, which likely explains the lower moisture uptake of paper C.

5.2. Moisture sorption hysteresis

Sorption hysteresis refers to the fact that the moisture content (MC) of a material depends not only on the current value of a_w but also on its preceding time history $a_w(t)$. As a consequence, the MC after moisture uptake (adsorption) differs from the MC after moisture loss (desorption), when an identical final a_w level is considered. This commonly results in the occurrence of a hysteresis loop when plotting MC against a_w,[64,65] as shown, *e.g.*, in Fig. 4.

Sorption hysteresis is widely encountered with, *e.g.*, natural fibers[36] and synthetic polymers.[66] Chen *et al.*[53] used molecular dynamics (MD) simulations and swelling experiments to show that hysteresis in cellulose arises from history-dependent hydrogen bond distributions during adsorption and desorption. Chen *et al.*[67] performed MD simulations that suggest that the presence of crystalline domains in amorphous cellulose reduces the sorption hysteresis. Salmén and Larsson[68] investigated sorption hysteresis in cellulose and a chemically partially modified form. They found that with increasing degree of modification, the softening temperature T_g decreased. Concurrently, moisture sorption hysteresis was reduced, disappearing entirely in the most modified samples. Similarly, increasing temperature reduced hysteresis. Weinmüller *et al.* showed that sorption hysteresis in hydrogels disappears when the rubber-to-glass transition temperature T_g falls below the sample temperature.[66] Zou *et al.* studied the interrelation of hysteresis and sorption-induced deformation.[69]

Fig. 6(b) shows that the sorption hysteresis of paper A disappears when a quantity of PEG300 with $\theta_{cs} \gtrsim 0.2$ g g^{-1} is added. This quantity is comparable to the moisture content of paper A at very high humidity $a_w \approx 1$, see Fig. 3(b). Due to the non-volatile nature of glycerol and PEG300, the co-solvents remain in the paper for the entire duration of the experiment and induce a persistent strain[28] on the order of $\Delta\varepsilon_{TD} \gtrsim 0.12$,

which is much larger than the hysteresis in ε_{TD} observed in Fig. 5. We hypothesize therefore that the co-solvents permanently occupy the adsorption sites in the cellulose fibers, the filling and emptying of which by water would otherwise give rise to hysteresis. Sala and Tomka observed an analogous disappearance of the sorption hysteresis in starch after addition of 10 wt% of glycerol, which reduced the glass transition temperature far below room temperature.[70]

5.3. Equilibrium moisture sorption of pure co-solvents

Glycerol has three hydroxyl groups (one per carbon atom), resulting in a higher number of hydrophilic sites per unit mass compared to EGOs (one ether group per two carbon atoms plus two terminal hydroxyl groups).[71] As the molecular weight of an EGO increases, the relative importance of its hydroxyl end-groups decreases. Hence, higher molecular weight EGOs are less hydrophilic and exhibit a lower aqueous solubility.[72] The different densities of polar groups explain why glycerol is able to absorb approximately twice as much water per unit mass as PEG300, as shown in Fig. 3(b).

5.4. Equilibrium moisture sorption of the two-component system paper + co-solvent

Adding 10 wt% glycerol to starch, which is chemically very similar to cellulose, can reduce the equilibrium MC,[73,74] although the MC of glycerol exceeds the MC of starch for all a_w values. In wood, the addition of EGOs can strongly reduce the moisture sorption capacity due to pore-filling and the much smaller expansion that is restricted by the structural rigidity of wood.[34] These systems are examples of scenario (2). In contrast, in all our experiments using glycerol and PEG300, the moisture sorption capacity of the two-component system did not fall measurably below that of the papers studied. The theoretical sorption model according to scenario (1) [lines in Fig. 6(a)] represents the experimental data for paper A + PEG300 very well; however, it slightly overpredicts the data for paper A + glycerol in Fig. 6(c). We hypothesize that the two effects ascribed to scenarios (2) and (3), *i.e.* the blockage of sorption sites by co-solvents and the availability of additional sorption sites due to the substantial swelling, might compensate each other, thereby explaining the unexpected success of scenario (1).

5.5. Pore-fiber transport rates of solutions

5.5.1. Impact of initial moisture/co-solvent content on pore-fiber transport rates of aqueous co-solvent solutions. Hermans and Vermaas studied the penetration of a glycerol/water mixture into a dry viscose fiber and observed the occurrence of two well-separated fronts.[75] They attributed the faster front to the penetration of water, which first needs to plasticize the fiber, before the second glycerol front can progress inward. This explains the existence of two timescales and makes it plausible that the initial moisture content of a cellulose fiber critically affects the pore-fiber transport rate of co-solvents as shown in Fig. 8. The same conclusion can also be drawn in the case of a non-zero initial co-solvent content in Fig. 9, because co-solvents swell cellulose fibers in an analogous fashion as water.

The characteristic swelling timescale $t_{0.63}$ for 40 wt% TEG in Fig. 7(c) is independent of a_w. This is attributed to the fact that the pore-fiber transport of the co-solvent is primarily influenced by the high initial water content of the solution.[40] A higher initial water concentration reduces the viscosity of the solution and, at the same time, efficiently plasticizes the fiber walls, thus promoting more expeditious pore-fiber transport.

The characteristic swelling timescale $t_{0.63}$ for 60 wt% TEG in Fig. 7(c) is roughly constant until $a_w = 0.5$ and then increases by a factor of 2. This seems to be inconsistent with all timescales remaining constant or decreasing in Fig. 7(b). The key is that above a water activity of 0.5, two separate relaxation times are required for an accurate BH fit of the experimental data and that the strain amplitude ratio A_{r2}/A_{r1} increases strongly with a_w, as shown in Fig. 7(d). This increases the relative importance of the slowest timescale t_{r2} and thus causes the increase of $t_{0.63}$. In contrast, a monotonic decrease of $t_{0.63}(a_w)$ is observed for EG in Fig. 8(c). The origin of this qualitative difference is unclear.

We note that the drying time t_{dry}, *i.e.* the time required for the excess water to evaporate, depends on a_w and is thus different for each of the experiments, as shown in Fig. 7. Prior to every experiment, we deposited a droplet of pure water (V = 1 μL) on a separate paper sample to determine its drying time t_{dry,H_2O}. Fig. S7(a) in the SI shows a plot of t_{dry,H_2O} as a function of a_w. In all cases, t_{dry,H_2O} exceeds 100 s. Fig. S7(b) shows that t_{dry} for aqueous EGO solutions is only very weakly dependent on the EGO concentration and the EGO MW. Therefore, we conclude that $t_d < t_{r2} < t_{dry}$ holds for all experiments in Fig. 7, whereas $t_{r1} < t_{dry}$ for $a_w \gtrsim 0.55$ and $t_{r1} > t_{dry}$ for $a_w \lesssim 0.55$. Karimnejad *et al.*[40] measured the effect of the co-solvent concentration on timescales t_d and t_{r1} at a fixed water activity. An approximately exponential dependence of t_d on the co-solvent concentration was found. Consequently, the values of t_d and t_{r2} in Fig. 7 are representative of the initial TEG concentration. However, the large values of t_{r1} for $a_w \lesssim 0.55$ are strongly affected by the evaporation of excess water and the concomitant increase in the TEG concentration.

The diffusion timescale of 60 wt% TEG in Fig. 7(b) at low water activities $a_w < 0.25$ is a factor of 4–8 faster than that for pure EG in Fig. 8(b), despite that MW(TEG) ≫ MW (EG) and that the viscosity μ (60 wt% TEG) is only about half of μ (EG). We interpret this to be a consequence of the plasticization of the fibers induced by the water present in the aqueous TEG solution.[75]

The diffusion timescale decreases by a factor of 3 in all EG experiments when approximately 0.04 g g^{-1} of liquid is present, as a consequence of either moisture sorption [Fig. 8(b)] or co-solvent deposition [Fig. 9(a)]. In both cases, an increase in the initial liquid content will increase the relaxation timescale t_{r1}. These observations suggest that the presence of moisture or EG both accelerate pore-fiber transport in an analogous fashion.

Fig. 9(c) shows that $t_{0.63}$ decreases with increasing $\theta_{cs,ini}$ for both EG and glycerol, indicating faster overall characteristic swelling due to co-solvent-induced softening of cellulose. A

higher water activity further accelerates the response. EG induces faster swelling due to its lower viscosity, smaller MW and weaker hydrogen bonding with cellulose. These properties enhance its diffusion and plasticization efficiency within the fiber network.

Wang and Darhuber introduced a phenomenological model for pore-fiber transport of co-solvents in paper.[39] They assumed that the pore-fiber transport rate depends on the solution viscosity, the effective permeability of the fiber wall, the difference in capillary pressures of pores and fibers and an empirical, concentration-dependent retardation factor $f(c)$. The data presented in Fig. 7–9 will be used to test the validity of their model and determine the values of the corresponding transport parameters.

5.5.2. Multi-component solutions. Surfactants are commonly added to inkjet printing inks to improve printability and increase imbibition rates into hydrophobic media.[76] Their presence can speed-up the pore-fiber transport of aqueous co-solvent solutions significantly.[40] Fig. 10(a) shows that this acceleration persists throughout the range of relative humidities studied. Consistent with Fig. 7(c), higher values of a_w drastically increase $t_{0.63}$.

Divalent metal salt solutions (so-called primer solutions) are frequently deposited on paper immediately before ink deposition to induce rapid flocculation of the colorant and latex particles suspended in the ink.[77,78] Fig. 10(b) shows that the addition of $MgCl_2$ strongly decreases the pore-fiber transport rates of 60 wt% TEG solutions by approximately a factor of 3. The same retardation effect has been observed by Stamm and Tarkov for imbibition of a saturated $MgCl_2$ solution into wood sections.[79] Andreasson *et al.* observed a decrease in the nanoscale pore radii of the fiber walls with increasing salt concentration, which they attributed to a decreased electrostatic repulsion.[80] Karlsson *et al.* reported that addition of salt has a significant impact on the water uptake capacity of cellulose nanofibrils.[81] We found that an important contribution to the retardation effect is the high sensitivity of the solution viscosity to c_{MgCl_2}, which increases by more than 60% in the concentration range studied, as illustrated in Fig. S9 of the SI. Analogous to the case of ternary solutions containing SDS above, higher values of a_w again significantly increase $t_{0.63}$. This behavior also persists for a quaternary aqueous solution of TEG, SDS and $MgCl_2$ (see Fig. S8 of the SI).

6. Conclusions

This manuscript provides a systematic evaluation of how water activity and the presence of co-solvents like glycerol and EGOs affect moisture uptake and the pore-to-fiber transport dynamics of model inks within cellulose-based papers. We infused papers with controlled amounts of co-solvent and measured their equilibrium moisture sorption for a wide range of water activities. This revealed that co-solvents increase the moisture uptake compared to untreated paper. Although co-solvents have a high affinity for paper, a non-interactive model based on a direct superposition of their individual sorption capacities represents the experimental data well. Interestingly, the deposition of co-solvents with a mass fraction of $\theta_{cs} \gtrsim 0.2\ g\ g^{-1}$ eliminates the sorption hysteresis observed for untreated paper. Furthermore, we found that increasing the ambient humidity or the initial co-solvent content accelerates the pore-to-fiber transport of the model inks in an analogous fashion.

6.1. Relevance to inkjet printing technology and beyond

Our results indicate that the co-solvent content and water activity have direct implications for print quality, ink-drying, sorption induced deformations of the paper substrate, and the long-term stability of inkjet-printed patterns. In inkjet printing, the quantity of ink deposited per area is typically smaller than the fiber holding capacity of the paper sheet. Therefore, co-solvents are not homogeneously distributed across a paper sheet, but are primarily located in the top part. As the regions containing co-solvents pick up more water than dry paper upon moisture sorption, this likely aggravates curl formation.[29]

An increase of the pore-fiber transport rate with increasing ambient humidity implies that the ink penetration depth into the paper is expected to increase for low humidity, because the water-*co*-solvent mixture remains in the inter-fiber pores for a longer time. By means of rapid drying, this undesirable effect can be reduced, as the water is removed. However, the remaining co-solvent may impart mobility to ink colorants, thus potentially inducing long-term color changes. The use of a volatile co-solvent such as EG would reduce this effect, at the expense of it being less effective in preventing inkjet nozzle clogging.

The findings of this study are relevant not only to inkjet printing but also for microfluidic systems and lab-on-a-chip technologies. In these applications, precise control of fluid transport through porous substrates or narrow channels is essential for achieving reliable diagnostics, chemical reactions, or biological assays.[82] The insights into how multicomponent solutions interact with hygroscopic porous media, such as cellulose fibers, and how ambient humidity modulates sorption and transport dynamics can inform the design of paper-based microfluidic devices. Moisture sorption can serve as an additional mechanism to enhance fluid control. By understanding the impact of moisture uptake, developers of low-cost, portable diagnostic tools can improve their reproducibility and stability under varying environmental conditions – challenges that are critical in point-of-care settings.

Author contributions

S. Karimnejad: investigation, data curation, methodology, visualization, formal analysis, writing – original draft, and writing – review and editing. A. A. Darhuber: conceptualization, investigation, methodology, formal analysis, supervision, funding acquisition, and writing – review and editing.

Conflicts of interest

There are no conflicts of interest to declare.

Data availability

The data supporting this article are included as part of the supplementary information (SI). Supplementary information is available. See DOI: https://doi.org/10.1039/d5sm00847f.

Acknowledgements

This work is part of an Industrial Partnership Program (i43-FIP) of the Foundation for Fundamental Research on Matter (FOM), which is part of the Netherlands Organisation for Scientific Research (NWO). This research programme is co-financed by Canon Production Printing, University of Twente, Eindhoven University of Technology, and the ''Topconsortia voor Kennis en lnnovatie (TKI)'' allowance from the Ministry of Economic Affairs. The authors are grateful to Nicolae Tomozeiu for the fruitful discussions.

References

1 S. D. Hoath, *Fundamentals of inkjet printing: the science of inkjet and droplets*, John Wiley & Sons, 2016.
2 P. J. Smith and A. Morrin, *Reactive Inkjet Printing: A Chemical Synthesis Tool*, Royal Society of Chemistry, 2017.
3 W. Zapka, *Handbook of Industrial Inkjet Printing: A Full System Approach*, Wiley-VCH, 2018.
4 M. McCormick-Goodhart and H. Wilhelm, *IS&T'S NIP16: Int. Conf. Digital Printing Technol.*, 2000, 74–77.
5 O. Högberg, M. Talaskivi and G. Ström, *IS&T'S NIP17: Int. Conf. Digital Printing Technol.*, 2001, 874–877.
6 M. McCormick-Goodhart and H. Wilhelm, *IS&T'S NIP17: Int. Conf. Digital Printing Technol.*, 2001, 179–185.
7 B. Rat, K. Možina, S. Bračko and A. Podlesek, *J. Imaging Sci. Technol.*, 2011, **55**, 50607.
8 A. Fricker, A. Hodgson, J. Townsend and C. Woods, *e-Preservation Sci.*, 2012, **9**, 60–66.
9 L. Salmén and E. Back, *Trans. VIth Fund. Res. Symp.*, 1977, 683–690.
10 B. V. Ramarao, *Studies in Surface Science and Catalysis*, Elsevier, 1999, 120, 531–560.
11 H. W. Haslach, *Mech. Time-Depend. Mater.*, 2000, **4**, 169–210.
12 C. Fellers, *Paper Products Physics and Technology*, de Gruyter, Berlin, 2009, pp. 109–143.
13 L. Solhi, V. Guccini, K. Heise, I. Solala, E. Niinivaara, W. Xu, K. Mihhels, M. Kröger, Z. Meng and J. Wohlert, *et al.*, *Chem. Rev.*, 2023, **123**, 1925–2015.
14 B. Lin, J. Auernhammer, J.-L. Schäfer, T. Meckel, R. Stark, M. Biesalski and B.-X. Xu, *Cellulose*, 2022, **29**, 1129–1148.
15 M. A. Hubbe, B. Sjöstrand, M. Lestelius, H. Håkansson, A. Swerin and G. Henriksson, *BioResources*, 2024, **19**, 6859–6945.
16 K. C. Yeh, J. M. Considine and J. C. Suhling, *Proc. Tappi Int. Pap. Phys. Conf.*, 1991, 695–711.
17 M. Lee, S. Kim, H.-Y. Kim and L. Mahadevan, *Phys. Fluids*, 2016, **28**, 042101.
18 J.-W. Rhim, *Food Sci. Biotechnol.*, 2010, **19**, 243–247.
19 W. J. Cousins, *Wood Sci. Technol.*, 1978, **12**, 161–167.
20 T. Uesaka, *J. Mat. Sci.*, 1994, **29**, 2373–2377.
21 H. Nanko and Y. Tada, *Proc. Int. Pap. Phys. Conf.*, 1995, 159–171.
22 A.-L. Erkkilä, T. Leppänen, M. Ora, T. Tuovinen and A. Puurtinen, *Nord. Pulp Pap. Res. J.*, 2015, **30**, 326–334.
23 W. Lu and L. A. Carlsson, *Mech. Time-Depend. Mater.*, 2001, **5**, 79–100.
24 T. Leppänen, J. Sorvari, A.-L. Erkkilä and J. Hämäläinen, *Model. Simul. Mat. Sci. Eng.*, 2005, **13**, 841–850.
25 P. Lipponen, T. Leppänen, J. Kouko and J. Hämäläinen, *Int. J. Solids Struct.*, 2008, **45**, 3596–3609.
26 S. Douezan, M. Wyart, F. Brochard-Wyart and D. Cuvelier, *Soft Matter*, 2011, **7**, 1506–1511.
27 E. Reyssat and L. Mahadevan, *Europhys. Lett.*, 2011, **93**, 54001.
28 C.-L. Wong, S. Wang, S. Karimnejad, M. Wijburg, H. Mansouri and A. Darhuber, *Soft Matter*, 2023, **19**, 1202–1211.
29 A. Maass and U. Hirn, *Mater. Des.*, 2024, **237**, 112593.
30 S. Magdassi, *The chemistry of inkjet inks*, World scientific, 2009.
31 C. Schmid, *The chemistry of inkjet inks*, World Scientific, Singapore, 2009, ch. 7.
32 J. Vonasek, M. Tuniuns and K. Rydinge, Method of preventing clogging of nozzles, US Pat. 5,781,214A, 1998.
33 J. Ljungdahl and L. A. Berglund, *Holzforschung*, 2007, **61**, 279–284.
34 A. Shomali, C. Zhang, B. Coasne, E. J. Schofield, B. Chabbert, D. Derome and J. Carmeliet, *Int. J. Bio. Macromol.*, 2025, **285**, 137661.
35 B. Saberi, Q. V. Vuong, S. Chockchaisawasdee, J. B. Golding, C. J. Scarlett and C. E. Stathopoulos, *Foods*, 2016, **5**, 1.
36 C. A. S. Hill, A. Norton and G. Newman, *J. Appl. Polym. Sci.*, 2009, **112**, 1524–1537.
37 L. Ninni, M. S. Camargo and A. J. A. Meirelles, *Thermochim. Acta*, 1999, **328**, 169–176.
38 M. G. Wijburg, S. Wang and A. A. Darhuber, *Colloids Surf., A*, 2023, **656**, 130268.
39 S. Wang and A. Darhuber, *Colloids Surf., A*, 2024, **682**, 132839.
40 S. Karimnejad, E. Gonnet, S. Wang, H. Mansouri, N. Tomozeiu and A. A. Darhuber, *Langmuir*, 2024, **40**, 19528–19537.
41 B. Spangenberg, C. F. Poole and C. Weins, *Quantitative Thin-Layer Chromatography*, Springer-Verlag, 2011.
42 *Paper-Based Optical Chemosensors*, ed. L. Feng, Elsevier, 2025.
43 *Paper Microfluidics*, ed. S. Bhattacharya, S. Kumar and A. K. Agarwal, Springer-Verlag, 2019.
44 *Absorbent Technology*, ed. P. Chatterjee and B. Gupta, Elsevier, 2025.

45 U. K. Krieger, F. Siegrist, C. Marcolli, E. U. Emanuelsson, F. M. Gøbel, M. Bilde, A. Marsh, J. P. Reid, A. J. Huisman, I. Riipinen, N. Hyttinen, N. Myllys, T. Kurtén, T. Bannan, C. J. Percival and D. Topping, *Atmos. Meas. Tech.*, 2018, **11**, 49–63.
46 S. P. Verevkin, D. H. Zaitsau, V. N. Emel'yanenko and A. A. Zhabina, *Fluid Phase Equilib.*, 2015, **397**, 87–94.
47 S. Basu, U. Shivhare and A. Mujumdar, *Drying Technol.*, 2006, **24**, 917–930.
48 J. J. v Laar, *Z. Phys. Chem.*, 1910, **72U**, 723–751.
49 J. J. Van Laar, *Z. anorg. allgem. Chem.*, 1928, **171**, 42–60.
50 H. Nakagawa and T. Oyama, *Frontiers Chem.*, 2019, **7**, 731.
51 A. Eliassi, H. Modarress and G. A. Mansoori, *J. Chem. Eng. Data*, 1999, **44**, 52–55.
52 K. W. Lang and M. P. Steinberg, *J. Food Sci.*, 1980, **45**, 1228–1230.
53 M. Chen, B. Coasne, R. Guyer, D. Derome and J. Carmeliet, *Nat. Commun.*, 2018, **9**, 3507.
54 A. Berens and H. Hopfenberg, *Polymer*, 1978, **19**, 489–496.
55 A. C. O'Sullivan, *Cellulose*, 1997, **4**, 173–207.
56 K. Hofstetter, B. Hinterstoisser and L. Salmén, *Cellulose*, 2006, **13**, 131–145.
57 A. Mihranyan, A. P. Llagostera, R. Karmhag, M. Stromme and R. Ek, *Int. J. Pharm.*, 2004, **269**, 433–442.
58 M. Ioelovich and A. Leykin, *BioResources*, 2011, **6**, 178–195.
59 M. E. Parker, J. E. Bronlund and A. J. Mawson, *Packag. Technol. Sci.*, 2006, **19**, 193–209.
60 A. H. Bedane, H. Xiao and M. Ei, *Adsorption*, 2014, **20**, 863–874.
61 P. A. C. Gane and C. J. Ridgway, *Nord. Pulp Paper Res. J*, 2009, **24**, 298–308.
62 Y. Hu and Q. Yu, *Geoenergy Sci. Eng.*, 2024, **236**, 212740.
63 T. Uesaka, *Handbook of physical testing of paper*, CRC Press, 2001, pp. 135–192.
64 S. Hou, J. Wang, F. Yin, C. Qi and J. Mu, *Wood Sci. Technol.*, 2022, **56**, 1087–1102.
65 J. G. Kapsalis, *Water Activity Influences on Food Quality*, ed. L. B. Rockland, G. F. Stewart, 1981, pp. 143–177.
66 C. Weinmüller, C. Langel, F. Fornasiero, C. Radke and J. Prausnitz, *J. Biomed. Mat. Res. A*, 2006, **77A**, 230–241.
67 M. Chen, B. Coasne, D. Derome and J. Carmeliet, *Cellulose*, 2020, **27**, 6945–6960.
68 L. Salmén and P. A. Larsson, *Carbohydr. Polym.*, 2018, **182**, 15–20.
69 Y. Zou, B. Maillet, P. Coussot and L. Brochard, *Phys. Rev. Res.*, 2025, **7**, 013205.
70 R. M. Sala and I. A. Tomka, *Angew. Makromol. Chem.*, 1992, **199**, 45–63.
71 L. Weng, C. Chen, J. Zuo and W. Li, *J. Phys. Chem. A*, 2011, **115**, 4729–4737.
72 J. A. Baird, R. Olayo-Valles, C. Rinaldi and L. S. Taylor, *J. Pharm. Sci.*, 2010, **99**, 154–168.
73 P. Myllärinen, R. Partanen, J. Seppälä and P. Forssell, *Carbohydr. Polym.*, 2002, **50**, 355–361.
74 J. I. Enrione, S. E. Hill and J. R. Mitchell, *J. Agric. Food Chem.*, 2007, **55**, 2956–2963.
75 P. H. Hermans and D. Vermaas, *J. Polym. Sci.*, 1946, **1**, 149–155.
76 B. Simončič and V. Rozman, *Colloids Surf., A*, 2007, **292**, 236–245.
77 A. Lundberg, J. Ortegren and O. Norberg, *J. Imaging Sci. Technol.*, 2011, **55**, 506051–506058.
78 Y. Yu and F. von Gottberg, *Proc. IS&T's NIP18: Int. Conf. Digital Printing Technol.*, 2002, 383–387.
79 A. J. Stamm and H. Tarkow, *J. Phys. Colloid Chem.*, 1950, **54**, 745–753.
80 B. Andreasson, J. Forsström and L. Wågberg, *Cellulose*, 2005, **12**, 253–265.
81 R.-M. P. Karlsson, P. T. Larsson, T. Pettersson and L. Wågberg, *Langmuir*, 2020, **36**, 12261–12271.
82 T. Akyazi, L. Basabe-Desmonts and F. Benito-Lopez, *Anal. Chim. Acta*, 2018, **1001**, 1–17.

